Harmonics Performance and System Stability Evaluation between 18-Pulse and LCL Filter Based Active Front End Converters under Weak Grid Condition

Kevin Lee† Wenxi Yao* Daniel Carnovale† Yuxi Huang*

† Electrical Sector
Eaton Corporation

*College of Electrical Engineering
Zhejiang University

Abstract - **Adjustable speed drives (ASDs) equipped with 18-pulse converter front end provide input disturbance rejection and clean power quality in various practical applications. In recent years, active front end (AFE) converters with LCL filters have gained popularity because of their four quadrant operational capability and low input current harmonics performance. However, the caveat exists that there are challenges for AFEs in achieving low harmonics and system stability under generator or weak grid environment. A systematic and quantitative comparison on input current harmonics performance and system stability between 18-pulse and AFE converters cannot be found in published literatures. In this paper, a robust 75hp (55kW), 480V, 60Hz 18-pulse clean power converter with "windmill" autotransformer topology is presented and analyzed, along with a state-of-the-art equivalent power level AFE with LCL filter. Theoretical investigation on AFE system stability with LCL filter using pole-zero map and Bode diagram is presented, followed by simulation studies under weak grid condition. Under normal and weak grid conditions, experimental tests with a 75hp (55kW) "windmill" 18-pulse clean power ASD and a 10kW AFE system with LCL filter are used for validating the accuracy and effectiveness of the analytical findings.**

I. INTRODUCTION

18-pulse converter based ASDs have been adopted successfully in a variety of industrial applications such as water management, wastewater treatment plants, HVAC, oil and gas fields with generators, where energy efficiency and harmonic mitigation for clean power are required. Properly designed 18-pulse converters can deliver true high power factor with low harmonics distortion, which prevents overheating of upstream transformers and overloading of breakers and feeders. As will be shown in this paper, 18-pulse system allows ASDs to be applied in generators and weak grid power systems. A 3-phase to 9-phase unity-gain autotransformer topology with ±20° phase shift between output voltages is first proposed [1]. The step-up and step-down 18-pulse autotransformer topologies with 40° phase shift between the output voltages are discussed [2-4]. The performances of a "windmill" topology based ASD with a novel 3rd harmonic computation method are quantified [5-6]. The winding current looping and sharing problems in early days have already been solved [7]. The challenging design problem becomes one of economics [8-9].

On the other hand, as power electronics technology proliferates, several breeds of harmonics reduction solutions such as AFE converter with LCL filter have been introduced in the market. Advantages of such an AFE system include regenerative energy flow, high input power factor, and low current harmonics under normal grid conditions in steady state. Limitations of voltage-oriented current control of AFE converters and damping issues are discussed [10-11], where it is pointed out that a stable operation is impossible outside a certain range of frequency ratios between LCL filter resonance and control frequencies. Furthermore, in the cases where a generator is used, or under weak grid scenario, serious resonance phenomenon can be produced. The interactions between LCL filter parameters, source impedance, and switching frequency can degrade the overall system stability margin. The characteristics of the weak grid and the associated challenges are summarized as follows:

1). Depending on the grid configuration, the grid impedance, which is mainly determined by power transformers and long distribution lines, may vary over a wide range. Because of these parameter variations, the fixed current controller loop gains in AFE can lead to system harmonic oscillation or instability;

2) The grid voltage at the point of common coupling (PCC) usually contains background harmonics, which are caused by the nonlinear load current flowing through the grid impedance. It has been indicated that even small levels of grid-voltage harmonics can greatly distort the injected grid current, resulting in poor power quality [12].

In order to suppress the current distortion caused by background harmonics in grid voltage, a dual loop, feed-forward function for grid-connected inverter with an LCL filter is evaluated [13]. Adopting the estimated grid impedance [14], the signal for the grid-voltage feed-forward is modified and the controller is adjusted with an adaptive rule to maintain a good phase margin or a high bandwidth. To improve the stability of the grid-connected inverter, an active damping control strategy based on virtual resistance in parallel with capacitor was presented in [15] as a mitigation solution. Leveraging the proportional and resonant current controller approach with feedforward, a trade-off enhancement between the harmonic-rejection capability and stability robustness is explored [16]. The effect of phase locked loop on system stability in LCL filter configuration is investigated [17]. From the pole-zero placement point of view, the potential instability

978-1-5090-2998-3/17/$31.00 ©2017 IEEE

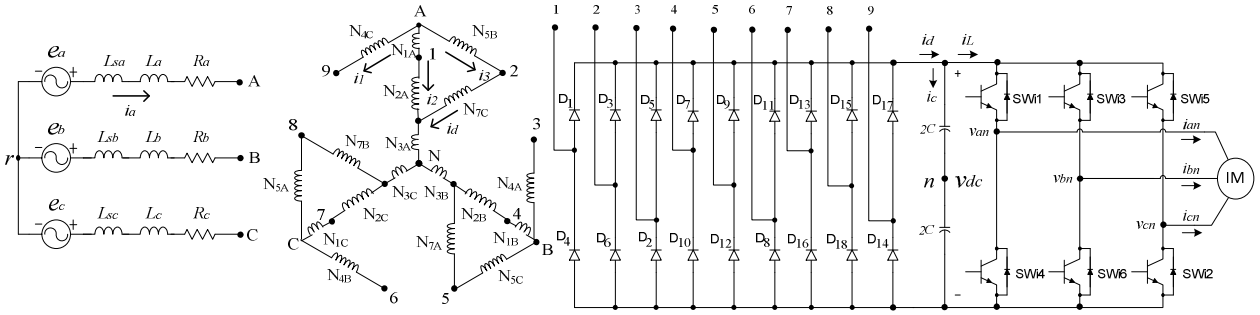

Figure 1: Overall circuit diagram of the "windmill" 18-pulse clean power adjustable speed drive system.

in case of low resonance frequency or weak grid with relatively large impedance results from the imperfect pole placement is researched [18]. A virtual impedance network is proposed [19] to improve harmonics rejection and stability margin under a weak grid condition.

Although there has been numerous researches conducted to address the AFE issues under weak grid conditions, there is a lack of effectiveness achieving stability consistently. A systematic and quantifiable harmonics performance and stability comparison between 18-pulse and AFE converters, especially under generator or weak grid does not exist in publications. One objective of this research is to fill that gap. In this paper, a cost effective "windmill" design of a state-of-the-art 3-phase to 9-phase 18-pulse autotransformer is utilized, where its kVA rating is only about 55% of the dc load power. The complete system model including the 18-pulse converter, inverter with SVPWM implementation, and the induction machine with a load range from 50% to 100% is simulated. For the AFE converter equipped with LCL filter, the system modeling with weak grid influence, LCL filter selection and controller designs are presented. The AFE system stability as a function of grid impedance variation is investigated. Through theoretical analysis and digital simulation, this paper quantifies the harmonics and system stability characteristics between 18-pulse and AFE converters under weak grid condition. The findings are applicable in the case of generators with larger impedance profile. Experimental setups including a 75hp (55kW) 18-pulse converter and an equivalent AFE with LCL filter are utilized for validating the analytical findings.

II. System Descriptions of the "Windmill" 18-Pulse Converter based ASD

In this 18-pulse converter system, a 3-phase input to 9-phase output autotransformer with 6 coils per phase is used to power a 9-phase ac to dc converter as shown in Fig. 1. The 3-phase input voltages feed through input line impedances (L_a and R_a) and source inductance (L_{sa}). It is assumed that the 3-phase input impedances are balanced, i.e., $L_a = L_b = L_c$, $R_a = R_b = R_c$ and $L_{sa} = L_{sb} = L_{sc}$. The 9-phase AC output voltages are fed to 3-phase rectifier bridges (D_1-D_{18}). The dc link voltage is smoothed by dc link capacitor (C). The inverter IGBTs (SW_{i1}-SW_{i6}) deliver 3-phase pulse width modulated (PWM) voltage waveforms with variable frequency and amplitude to the IM load.

The input 3-phase voltages are supported by coils N_{1A}, N_{2A}, N_{3A} for phase A, N_{1B}, N_{2B}, N_{3B} for phase B, and N_{1C}, N_{2C}, N_{3C} for phase C. Terminals A, B and C represent the input voltage connection points. Fig. 2 illustrates terminals 1–9 voltages which represent a 40° increment in phases.

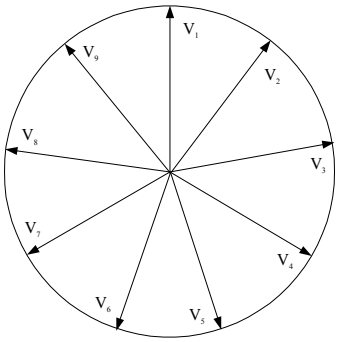

Figure 2: Nine-phase output voltages in the 18-pulse ASD system.

A delta winding in each phase is arranged to allow circulation of the required harmonic currents, but avoids circulation of the fundamental current. For instance, N_{5B} and N_{7C} are each equal in turns to the sum of turns N_{1A} and N_{2A}. The output voltages in terminals 1 and 2 are expressed as in Eqs. (1) and (2). Other voltages are calculated using the vector algebra respectively.

$$V_{1N} = V_{AN} \text{ x } \frac{N_{2A} + N_{3A}}{N_{1A} + N_{2A} + N_{3A}} \quad (1)$$

$$V_{2N} = V_{AN} + V_{BN} \text{ x } \frac{N_{5B}}{N_{1B} + N_{2B} + N_{3B}} \quad (2)$$

One important metric to evaluate the 18-pulse system cost is to calculate the equivalent transformer kVA power rating relative to the output dc power. Table 1 shows each calculated coil current in relation to the dc link current. The average dc output voltage of a 9-phase bridge rectifier fed by the "windmill" transformer is expressed in Eq. (3), which is about 4.2% higher than that of a 3-phase bridge.

$$V_{DC,"windmill"} = \frac{18\sqrt{2}}{\pi} \sin\frac{\pi}{9} \cdot \frac{\sin 60°}{\sin 80°} V_{L\text{-}N} = 2.44\ V_{L\text{-}N} \quad (3)$$

TABLE I. THE "WINDMILL" 18 PULSE CURRENT RATIO: I_{RMS} / I_{DC}.

Phase A		Phase B		Phase C	
Turns	I_{RMS} / I_{DC}	Turns	I_{RMS} / I_{DC}	Turns	I_{RMS} / I_{DC}
N_{1A}	0.486	N_{1B}	0.486	N_{1C}	0.486
N_{2A}	0.2	N_{2B}	0.2	N_{2C}	0.2
N_{3A}	0.2	N_{4B}	0.2	N_{4C}	0.2
N_{4A}	0.435	N_{5B}	0.435	N_{5C}	0.435
N_{5A}	0.324	N_{6B}	0.324	N_{7C}	0.324
N_{7A}	0.2	N_{7B}	0.2	N_{7C}	0.2

Where $V_{L\text{-}N}$ is the source line-to-neutral voltage $V_{L\text{-}N}$. As can be observed in Table I, full input line current does not flow through any winding. Total transformer kVA is obtained from closed form or computer solutions. In the "windmill" design the transformer kVA rating is about 55% of the dc load kW [6] as shown in Eq. (4).

$$\frac{Transformer\ kVA}{DC\ Load\ kW} \cong 0.55 \tag{4}$$

The harmonics cancellation in Fig.1 is described in Eqs. (5-8) using phase "A" various winding currents as an illustration. The 1st, 7th, 13th, … harmonics are positive sequence components, while 5th, 11th, 17th, … are in negative sequence. The 3rd harmonic current flows in the delta winding.

$$i_1 = I_{11}\sin(\omega t) + \sum_{n=5,7,11,13,17,19\ldots}^{\infty} I_n \sin(n\omega t) \tag{5}$$

$$\begin{aligned} i_2 = {} & I_{21}\sin(\omega t) - I_d \sin(3\omega t) + \\ & \sum_{n=7,13,19\ldots}^{\infty} I_n \sin(n(\omega t + 20°) - 20°) + \\ & \sum_{n=5,11,17,\ldots}^{\infty} I_n \sin(n(\omega t + 20°) + 20°) \end{aligned} \tag{6}$$

$$\begin{aligned} i_3 = {} & I_{31}\sin(\omega t) + I_d \sin(3\omega t) + \\ & \sum_{n=7,13,19\ldots}^{\infty} I_n \sin(n(\omega t + 40°) - 40°) + \\ & \sum_{n=5,11,17,\ldots}^{\infty} I_n \sin(n(\omega t + 40°) + 40°) \end{aligned} \tag{7}$$

The 3rd, 5th, 7th, 11th, and 17th harmonic components from i_1, i_2, and i_3 are added to zero in i_a as expressed in Eq. (8). The remaining two phases on the input are similar with only 17th, 19th harmonic components and their multiples left.

$$i_a = I_1\sin(\omega t) + I_{17}\sin(17\omega t) + I_{19}\sin(19\omega t) + \ldots \tag{8}$$

In this paper, the weak grid and various source voltage characteristics are built into source inductances of L_{sa}, L_{sb}, L_{sc}, and source voltages of e_a, e_b, e_c. Unlike an AFE based ASD, the "windmill" 18-pulse converter has uncontrolled input rectifier circuit with a dc link energy storage capacitor support, thus inherently stable. As a matter of fact, in the presence of a generator or weak grid, the 18-pulse ASD system has even improved current harmonic performance as presented in this paper.

III. ANALYTICAL MODEL OF THE AFE WITH LCL FILTER UNDER WEAK GRID CONDITION

The AFE circuit configuration is shown in Fig. 3 (a), which includes a three-phase converter IGBT bridge (Q_{g1}-Q_{g6}) to allow bi-directional power flow and a 3-phase LCL filter for suppressing high switching frequency components feeding back to the source while reducing lower order input current harmonics. Fig. 3 (b) illustrates the LCL equivalent circuit, where L_f is the converter side inductance, L_g is the grid side inductance, L_s is the grid inductance which can represent weak grid, C_f is the filter capacitor and R_c is the damping resistor.

The transfer functions of the LCL filter in Fig. 3 are described in Eqs. (9) and (10). The converter side current is used for the feedback control, thus, Eq. (9) is used in the control system design and the system stability assessment. Meanwhile, the transfer function of the grid current in Eq. (10) can be applied in the analysis on how LCL filter can suppress the switching frequency harmonics in the grid current [20].

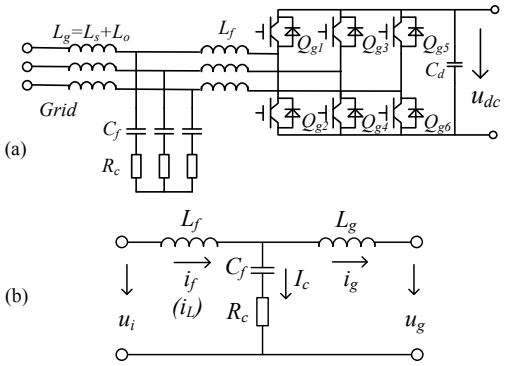

Figure 3: (a). AFE circuit; (b) LCL filter equivalent circuit.

$$G_{if/ui}(s) = \frac{i_L(s)}{u_i(s)} = \frac{s^2 L_g C_f + sC_f R_c + 1}{s^3 L_f L_g C_f + s^2(L_f + L_g)C_f R_c + s(L_f + L_g)} \tag{9}$$

$$G_{ig/ui}(s) = \frac{i_g(s)}{u_i(s)} = \frac{sC_f R_c + 1}{s^3 L_f L_g C_f + s^2(L_f + L_g)C_f R_c + s(L_f + L_g)} \tag{10}$$

To investigate the weak grid influences on AFE system stability, we rearrange Eq. (9) to obtain Eq. (11) in the form of natural frequency ω_n and damping ratio ξ as represented in Eq. (12). When LCL filter values including the damping resistor R_c are fixed, it can be seen that the system damping depends on L_g, which is a function of the grid inductance. Furthermore, the resonant frequency (f_{res}) of the overall LCL filter interacting with the grid inductance is recommended to satisfy Eq. (13) for maintaining stability [21], where f_g is the grid frequency, and f_{SW} is the converter switching frequency.

$$G_{iL/ui}(s) = \frac{1}{(L_f + L_g)} \cdot \frac{1}{s} \cdot \frac{s^2 L_g C_f + sC_f R_c + 1}{\left(\frac{s}{\omega_n}\right)^2 + 2\xi\omega_n s + 1} \tag{11}$$

$$\omega_n = \sqrt{\frac{L_f + L_g}{L_f L_g C_f}}, \quad \xi = \frac{1}{2} C_f R_c \sqrt{\frac{L_f L_g C_f}{L_f + L_g}} \tag{12}$$

$$f_{sw}/6 < f_{res} < 0.5 f_{sw} \tag{13}$$

While keeping the LCL parameters unchanged, it can be seen that increasing R_c in the s^2 coefficient can improve the system damping, which is the basic principle of passive damping. When increasing R_c can move the zeros and poles of system inward, away from unit circle boundary with increased damping effect, it also increases the additional loss.

The 75hp (55kW) AFE system has the parameters: L_g = 600μH, L_f = 700μH, C_f = 15μF, and R_c = 0.75Ω. Fig. 4 shows the pole-zero map of the current controlled closed loop transfer function from Eq. (9), where the weak grid inductance varies from L_g = 0.6mH to 2.6mH. The AFE switching frequency is 3.6kHz with a double update sampling frequency at 7.2kHz. As the weak grid inductance increases, the dominant poles become slower, while the resonant poles move outwards of the unit circle. As a result, the stability of the AFE system deteriorates.

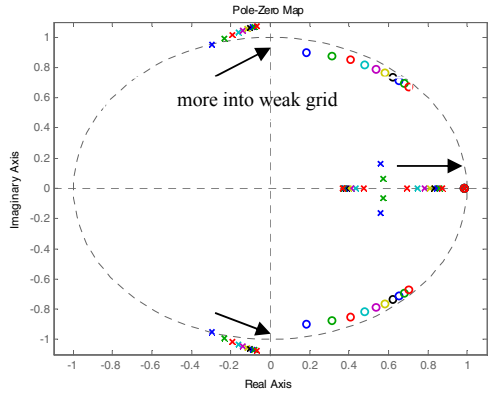

Figure 4: Pole zero map of 75hp (55kW) AFE with LCL filter when L_g changes from 0.6mH to 2.6mH.

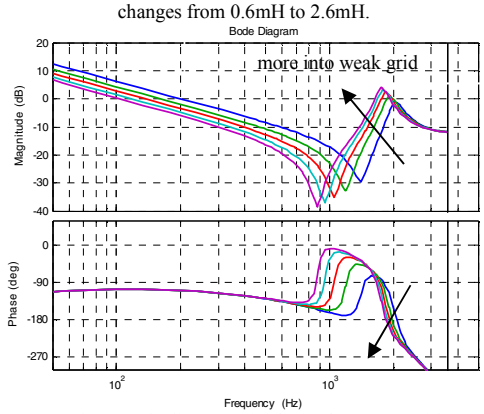

Figure 5: Open loop Bode diagram of 75hp (55kW) AFE with LCL filter when L_g changes from 0.6mH to 2.6mH.

The same conclusion can be drawn in the corresponding Bode plot in Fig. 5. The resonant frequency reduces as the weak grid deepens, its peak value increases above zero dB in magnitude and the phase margin degrades further. The unstable trend is more pronounced in industrial applications, where the switching frequency cannot be arbitrarily set to a higher value for reduced system losses and manageable electromagnetic interference (EMI).

IV. Simulation Results and Analysis

Simulation studies of the 18-pulse and AFE systems using PSIM and Matlab/Simulink have been conducted to evaluate the system stability and input current harmonics performance. A quantitative comparison has been made between a 75hp (55kW) 18-pulse converter and an AFE based ASD with LCL filter. The operating point parameters of the 18-pulse converter consist of L_a = 525μH, C = 2800μF, and inverter driven IM load. The 75hp (55kW) AFE based ASD with LCL filter has L_g = 600μH, L_f = 700μH, C_f = 15μF, and R_c = 0.75Ω.

Fig. 6 depicts the simulation results of the 18-pulse system with an input current of 69.3A, and dc link voltage at ~648V under a 525μH weak grid condition. The input current total harmonic distortion (THD) is 3.67% which is better than 4.9% under normal grid condition, with an unchanged power factor of 0.98 in both cases.

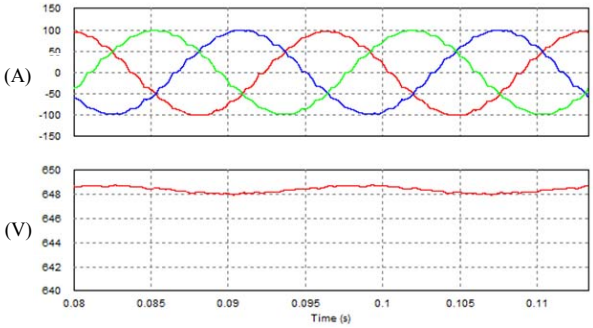

Figure 6: 75hp (55kW) 18-pulse system input currents, dc link voltage at 69.3A load under weak grid condition.

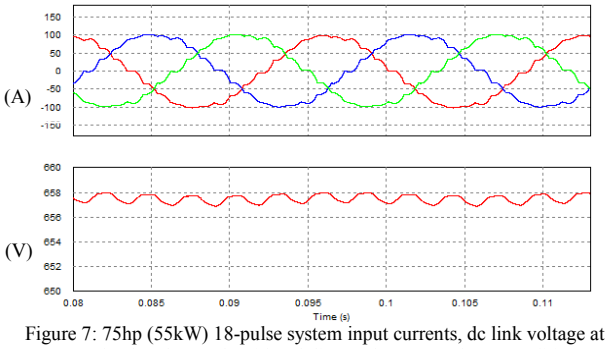

Figure 7: 75hp (55kW) 18-pulse system input currents, dc link voltage at 70.0A load under weak grid and distorted source voltage condition.

Fig. 7 illustrates the simulation results of the same system under a distorted source voltage containing 3.6% voltage THD, with an input current of 70.0A, and dc link voltage of ~657V. The 6th harmonic ripple on the dc link voltage is caused by the 5th and 7th source voltage harmonics. The input current THD is 5.76% which is marginally worse than 4.9% under normal grid condition, with an unchanged power factor of 0.98.

Fig. 8 shows the simulation results of a 75hp (55kW) AFE system with an input current of 70A, dc link voltage of 720V under normal grid condition. The input current THD is 4.19%.

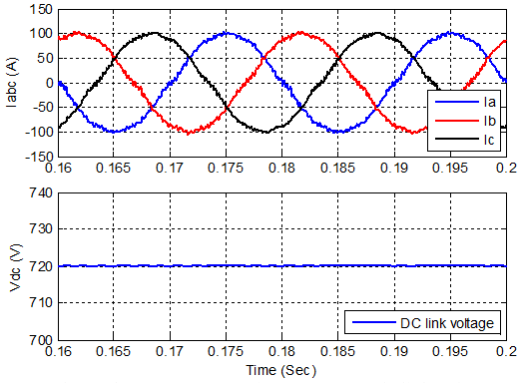

Figure 8: 75hp (55kW) AFE system input currents, dc link voltage at 70A load under normal grid condition.

Fig. 9 illustrates the simulation results of the same system under weak and distorted source voltages containing a 525μH weak grid, 2% of 5th and 7th, 1% of 11th and 13th voltage harmonics. The system becomes unstable with an uncontrollable input current of ~105A instead of 70A, and dc link voltage at ~702V, off from a set point of 720V. The AFE system instability introduces an input current THD of ~19.6%.

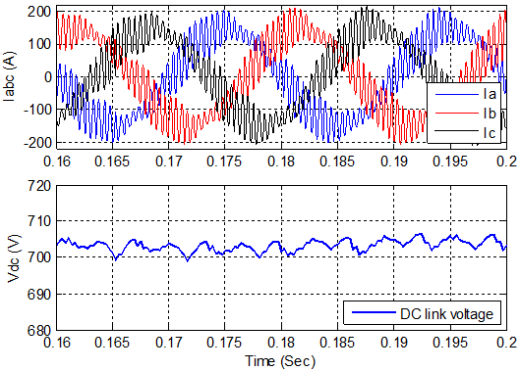

Figure 9: 75hp (55kW) AFE system input currents, dc link voltage at ~105A load under weak & distorted grid condition.

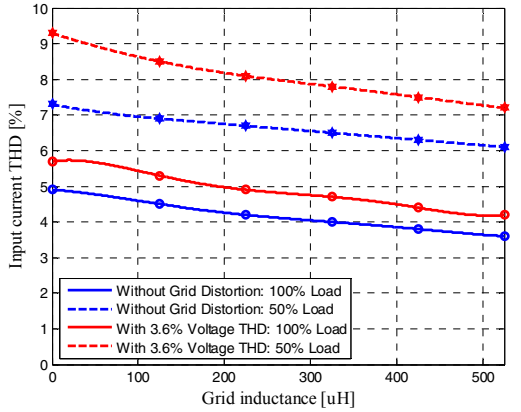

Figure 10: 75hp (55kW) 18-pulse system: Input currents variation with grid inductance and load, with and without grid voltage distortions.

The trend analysis on input current harmonics performance has been conducted, with and without a distorted source voltage of 3.6% THD. For the 18-pulse converter, Fig. 10 demonstrates how the current THD varies as weak grid develops at both full and half loads. The weaker the grid, the better the input THD performance in the case of the 18-pulse converter, which is robust and suitable in weak grid and high impedance generator environments. In the case of AFE system as shown in Fig. 9, the instability issue under a weak grid makes the trend analysis less meaningful.

V. Mitigation Solution to AFE Instability Issue under Weak Grid Condition

The Fast Fourier Transform (FFT) of the AFE input current waveform of Fig. 9 is depicted in Fig.11. Under the weak grid condition, the resonant frequency becomes 1.978kHz based on Eq. (10) with the defined parameters in Section IV.

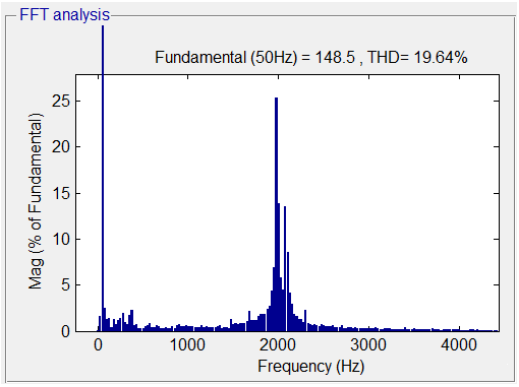

Figure 11: 75hp (55kW) AFE system input current harmonic profile under weak & distorted grid condition in Figure 9.

It can be observed that the harmonic component at the resonant frequency dominates the harmonic performance. The inner current controller loop with an outer dc link voltage regulator is used in the analysis. Fig. 12 illustrates the current controller block diagram in discrete z-domain, where i_r is the reference signal for i_f in Fig. 3 generated from the outer dc link voltage regulator, G_{AFE} represents the transfer function in Eq. (9), and G_c is the current controller.

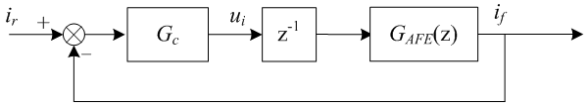

Figure 12: Current control block diagram in 75hp (55kW) AFE system.

In order to solve the instability problem under the weak grid condition, the current controller bandwidth is reduced from 220Hz to 110Hz as shown in Fig. 13. While the phase profiles remain the same in both cases, the harmonic amplitude at the resonant frequency is attenuated by ~6dB.

Fig. 14 demonstrates the improved input currents in the simulation results at 70A RMS and a dc link voltage of 720V. The amplitude of the input current at the resonant frequency is attenuated effectively. Fig. 15 is the corresponding FFT harmonics spectrum with an input current THD of 3.47%.

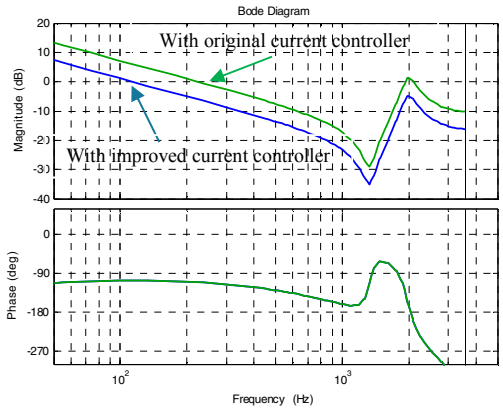

Figure 13: Open loop Bode diagram of 75hp (55kW) AFE with improved current controller bandwidth under the weak grid condition.

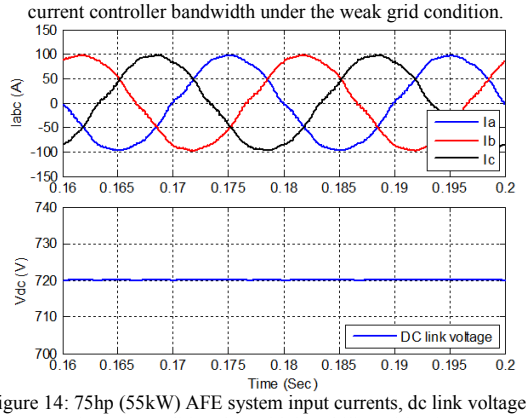

Figure 14: 75hp (55kW) AFE system input currents, dc link voltage at Figure 9 condition, but with instability mitigation.

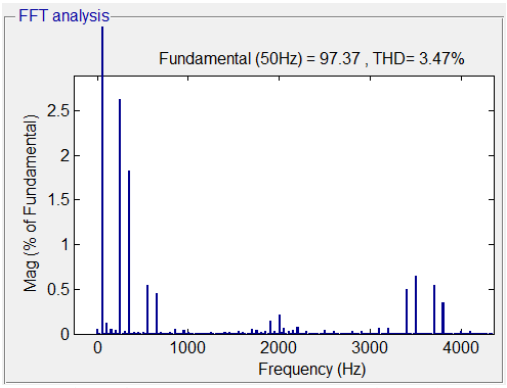

Figure 15: 75hp (55kW) AFE system input current harmonic profile at Figure 9 condition, but with instability mitigation.

VI. Experimental Verification

The 75hp (55kW), 480V, 60Hz "windmill" 18-pulse converter based ASD is put into test for its performance under the weak grid condition. The experimental setup with following parameters: L_a = 525µH, C = 2800µF is shown in Fig. 16. Under normal grid condition (source impedance of 5.1% in 300KVA base) at the testing facility, Fig. 17 shows the input line-neutral voltages which contain 2.3% THD, and input currents with 6.1% THD respectively. Under the weak grid condition (18% in 300KVA base), Fig. 18 depicts the input voltages with 4.1% THD, and currents with 4.7% THD.

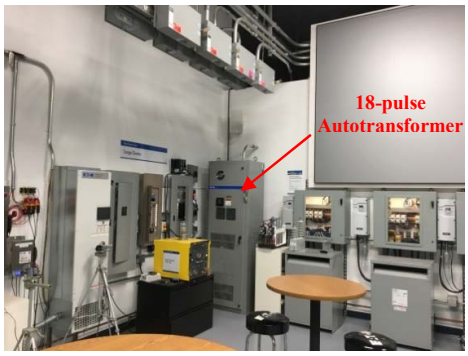

Figure 16: Experimental "windmill" 18-pulse ASD system setup.

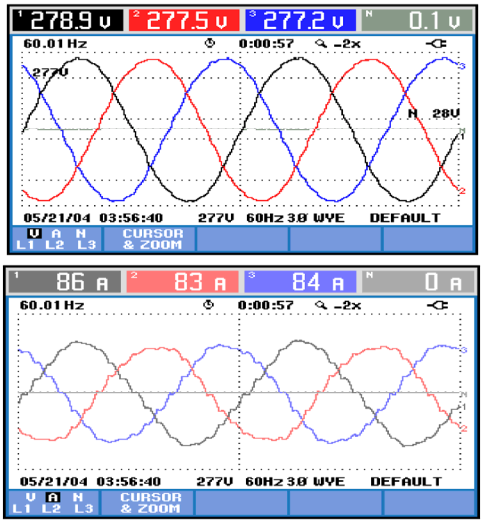

Figure 17: Experimental 18-pulse input voltages (upper window) and currents (lower window) under normal grid condition.

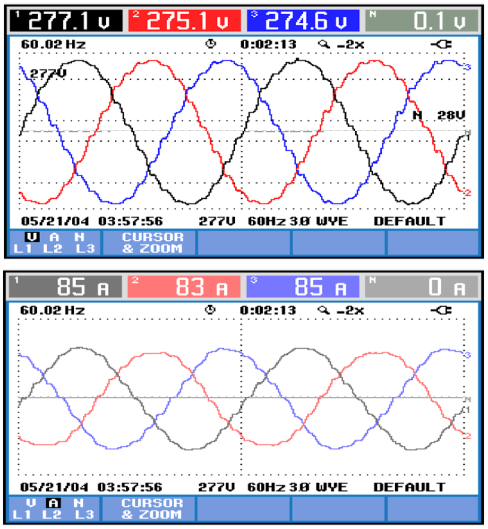

Figure 18: Experimental 18-pulse input voltages (upper window) and currents (lower window) under weak grid condition.

Table 2 lists the measurement results on the 18-pulse system at the testing facility. Under normal grid condition without load, the power distribution system already has a background voltage THD of 1.9%. Under normal grid at 100% load, it becomes 2.3%, then worsens to 4.1% under the weak grid. Although there is variation between real source and ideal source inductance values, the simulation and experimental results agree quite well in predicting the trend.

TABLE II. EXPERIMENTAL RESULTS OF THE "WINDMILL" 18-PULSE CONVERTER UNDER NORMAL GRID AND WEAK GRID CONDITIONS.

THD (%)	Normal Grid, 100% Load	Weak Grid, 100% Load
Source Voltage	2.3	4.1
Input Current	6.1	4.7
THD (%)	Normal Grid, 50% Load	Weak Grid, 50% Load
Source Voltage	2.0	3.7
Input Current	9.5	8.3

Comparing the results between Figs. 17 and 18, the source voltage THD increases under the weak grid condition, however, the input current waveforms improve with less harmonic distortion.

A scaled down 10kW AFE system in the experimental validation is conducted, which has L_g = 2mH, L_f = 2.2mH, C_f = 6μF, and L_s = 2mH in the case of the weak grid condition. The measured dc link voltage (100V/div) and input current (5A/div) are recorded in Fig. 19 under the normal grid condition. The corresponding input current FFT profile is analyzed in Fig. 20 with a THD of 2.96%. The current PI controller gains are K_p = 0.2 and K_i = 600 respectively. Notice that the resonant frequency is not dominant in the FFT.

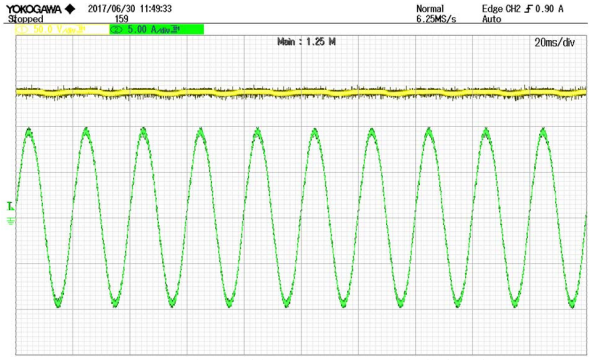

Figure 19: AFE experimental input current and dc link voltage under normal grid condition.

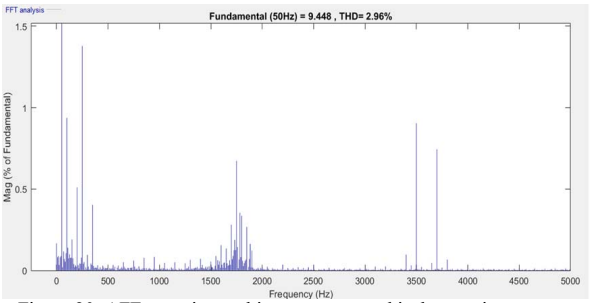

Figure 20: AFE experimental input current and its harmonic spectrum under normal grid condition.

Under the weak grid condition, the same variables of the measured dc link voltage and input current are captured in Fig. 21. The corresponding input current FFT profile is depicted in Fig. 22 with a THD of 32.27%. The current PI controller gains remain the same. The resonant frequency becomes dominant as compared to the switching frequency of 3.6kHz. With a significant current THD degradation, the system is indeed at the border line of becoming unstable. A slight increase for K_p causes the AFE to totally lose control. In order to improve the system stability, the current controller bandwidth is reduced as described in Section 5, such that the input current waveform quality in Fig. 19 is achieved.

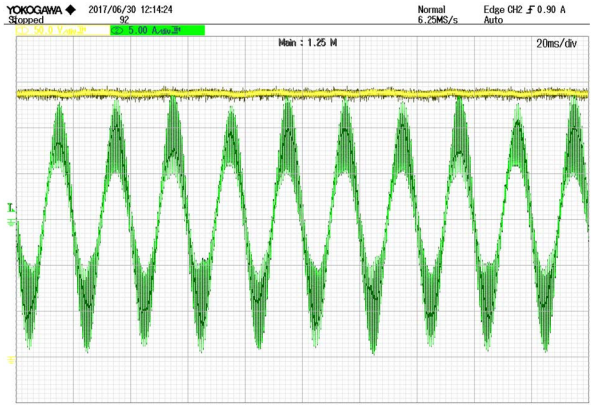

Figure 21: AFE experimental input current and dc link voltage under weak grid condition.

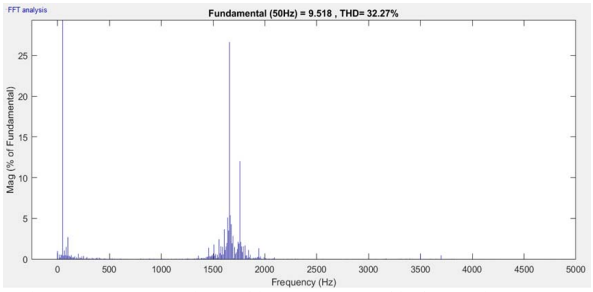

Figure 22: AFE experimental input current and its harmonic spectrum under weak grid condition.

With respect to the harmonic requirements, IEEE519-2014 guidelines [22] clearly mention that harmonics at the input of ASDs are not relevant and that it should be measured at a public utility system and on the medium voltage (MV) side for industrial applications. Also, the harmonics are evaluated on an annual basis and should be a statistical result and not an instantaneous measurement. In this paper, the focus is not only on comparing the harmonic characteristics between 18-pulse and AFE converters, but also more importantly emphasizing the impact on system stability under weak grid condition.

VII. CONCLUSIONS

In this paper, a quantitative harmonics performance and system stability evaluation is presented between a "windmill" 18-pulse and a LCL filter based AFE Converter under normal and weak grid conditions. It is shown through modeling,

analysis, simulation, and experimentation that the 18-pulse topology, when placed in weaker grid, can achieve better input current THD and maintain system operational stability. This performance level and robustness prove to be especially invaluable in power distribution systems where high impedance generators are used in remote locations where a stiff source is not available. Although LCL filter based AFE can provide four-quadrant power flow and lower order harmonics mitigation under normal grid conditions, it can be very vulnerable to become unstable under weak grid condition interacting with LCL filter parameters, current controller bandwidth and switching frequency. Since the grid impedance is often unknown, it is challenging to design an AFE system with various LCL filter parameters at different power levels to deliver a stable operation under weaker grid condition. Theoretical analysis on AFE system stability with LCL filter using pole-zero map, root locus and Bode diagram is explored. Simulation studies in both 18-pulse and AFE converters have been conducted. Furthermore, for the 18-pulse configuration, the trend study of input harmonics performance as functions of source inductance, harmonics and load is investigated. In addition to include optimal control strategies in the reference section for solving the AFE stability issue under weak grid condition, a mitigation solution involving the current controller bandwidth is proposed in this paper. Experimental tests on a 75hp (55kW) "windmill" 18-pulse and a 10kW AFE system are used for validating the accuracy and effectiveness of the analysis.

REFERENCES

[1] D. A. Paice, "Multi-pulse converter system," U. S. Patent #4,876,634, Oct. 1989.

[2] D. Zhou, G. L. Skibinski, and N. Guskov, "Nine phase transformer," U. S. Patent #6,335,872, Jan. 2002.

[3] P. Hammond, "Autotransformer," U.S. Patent #5,619,407, Apr. 1997.

[4] D. A. Paice, "Wye connected 3-phase to 9-phase auto-transformer with reduced winding currents," U.S. Patent #6,191,968B1, Feb. 2001.

[5] K. Lee, J. E. Armes, D. A. Paice, "Evaluation of 3-phase to 9-phase transformer, 18-Pulse converter, and adjustable speed drive, including novel third harmonic calculations", IEEE Applied Power Electronics Conference and Exposition, pp. 781-789, 2007.

[6] K. Lee, J. E. Armes, D. A. Paice, "The windmill topology: Evaluation of adjustable speed drive systems", IEEE Industry Applications Magazine, March 2009.

[7] G. L. Skibinski, N. Guskov, and D. Zhou "Cost effective multiple pulse transformer solutions for harmonic mitigation in ac drives". IEEE 38th IAS Conference, vol. 3, pp. 1488-1497, Oct. 2003.

[8] D. A. Paice, "Power electronic converter harmonics: Multipulse methods for clean power," IEEE Press, 1996.

[9] D. A. Paice, "Clean power electronic converters: Engineering design and application guides," Paice & Associates, Inc., 2005.

[10] J. Dannehl, C. Wessels, and F. W. Fuchs, "Limitations of voltage-oriented PI current control of grid-connected PWM rectifiers with LCL filters," IEEE Transactions on Industrial Electronics, vol. 56, no. 2, pp. 380-388, 2009.

[11] S. G. Parker, B. P. McGrath, and D. G. Holmes, "Regions of active damping control for LCL filters," IEEE Transactions on Industry Applications, vol. 50, no. 1, pp. 424-432, Jan./Feb. 2014.

[12] D. Yang, X. Ruan, and H. Wu, "Impedance shaping of the grid-connected inverter with LCL filter to improve its adaptability to the weak grid condition," IEEE Transaction on Power Electronics, vol. 29, no. 11, pp: 5795-5805, Nov. 2014.

[13] X. Wang, X. Ruan, and S. Liu, "Control strategy for grid-connected inverter to suppress current distortion effected by background harmonics in grid voltage," Proceedings of the CSEE, vol. 31, no. 6, pp. 7-14, 2011.

[14] J. Xu, S. Xie, T. Tang, "Improved control strategy with grid-voltage feedforward for LCL-filter-based inverter connected to weak grid," IET Power Electronics, vol. 7, issue 10, pp. 2660-2671, 2014.

[15] X. Chen, C. Y. Gong, H. Z. Wang, and L. Cheng, "Stability analysis of LCL-type grid-connected inverter in weak grid systems," International Conference on Renewable Energy Research and Applications (ICRERA), pp. 1-6, 2012.

[16] W. Li, "Research on suppressing harmonic and unbalanced injected grid currents caused by grid voltages for the three-phase LCL-type grid-connected inverter," Ph.D. thesis, Huazhong University of Science and Technology, Wuhan, China, 2014.

[17] H. Wu, X. Ruan, and D. Yang, "Research on the stability caused by phase-locked loop for LCL-type grid-connected inverter in weak grid condition," Proceedings of the CSEE, vol. 34, no. 30, pp. 5259-5268, 2014.

[18] M. Xue, Y. Zhang, F. Liu, and Y. Kang, and Y. Yi, "Optimized pole and zero placement with state observer for LCL-type grid-connected inverter," IEEE ECCE, pp. 377-382, 2011.

[19] D. Yang, X. Ruan, and H. Wu, "Using virtual impedance network to improve the control performances of LCL-type grid-connected inverter under the weak grid condition," IEEE APEC, pp. 3048-3054, 2014.

[20] Y. Tang, L. Huang, and G. Zhao, "Resonant feed forward control for LCL-type grid-tied inverters in weak grid condition," IEEE ECCE, Sept. 2016.

[21] M. Lu, Z. Xin, X. Wang, R. N. Beres, and F. Blaabjerg, "Extended stable boundary of LCL-filtered grid-connected inverter based on an improved grid-voltage feedforward control," IEEE ECCE, Sept. 2016.

[22] IEEE Std. 519-2014, "IEEE recommended practice and requirements for harmonic control in electric power systems," 2014.